Deformation, Orientation, and Scattering from Polymer Chains in Shear Flow. A Brownian Dynamics Simulation Study

J. J. López Cascales, S. Navarro, and J. García de la Torre*

Departamento de Quimica Fisica, Universidad de Murcia, 30071 Murcia, Spain

Received November 13, 1991; Revised Manuscript Received February 21, 1992

ABSTRACT: The conformation of polymer chains in shear flow is simulated by applying the Brownian dynamics technique to bead-and-spring model chains without and with hydrodynamic interaction (HI). The deformation of the chain is characterized as the variation of the components of the square radius of gyration tensor with shear rate. Our simulation results for the increase in the radius of gyration agree with early results without HI and confirm recent renormalization group predictions with HI. Available experimental data from neutron scattering are discussed in terms of these theoretical and simulation results. We predict the scattering intensities for a simulated experiment in which the orientation of the scattering vector with respect to the flow direction is continuously varied. We also consider the deformation and orientation of subchains in the polymer, looking at the stretching and orientation of the individual springs in the model as functions of their position along the chain.

Introduction

The theoretical prediction of rheological properties of dilute polymer solutions becomes very difficult when relevant effects such as hydrodynamic interaction (HI) are properly considered. As an alternative to analytical developments, Brownian dynamics (BD) simulation has emerged as a powerful tool in the past few years, enabling in some cases the confirmation of theoretical results and, more interestingly, novel predictions in others. Some examples of BD simulations of polymer chains in flow are presented in refs 1–9. Concretely, we[6] carried out a BD simulation of polymer conformation in shear flow looking for the effect of HI on the dimensions of bead-and-spring chains. The problem is of practical relevance, since the determination of experimental data has already been achieved.[10] We confirmed theoretical predictions for the no-HI case[10-13] and obtained new results from simulations with HI. We made a somewhat rough analysis of the HI results because no general laws were available.

Quite recently, Wang[14] has published theoretical results for the radius of gyration (and its components) of the bead-and-spring chains in shear flow with HI. This author finds that polymer deformation, expressed as the relative change in dimensions, is proportional to the square of the dimensionless shear rate, β, which combines shear rate and the zero-shear-rate intrinsic viscosity (see eq 8 below). It is interesting to employ BD simulation to verify that prediction. Then, we have repeated our simulations in ref 6, running longer trajectories in order to get better statistical quality of the data. We obtain in the simulation not only the whole radius of gyration but also the complete gyration tensor. The resulting data are now analyzed in terms of β^2 laws, and the proportionality constants are compared with those reported by Wang.[14]

The statistical shape of the polymer chain could be in principle determined from radiation scattering with two-dimensional detectors, varying the scattering geometry, i.e., both the modulus of the scattering vector as well as its orientation with respect to the direction of flow. The shape can be visualized as a polar plot of chain size in a given direction. From our Brownian dynamics results, we predict such shape functions, which are in turn used to predict the variation of scattering intensities with varying orientation. Indeed, we predict the outcome of a hypothetical scattering experiment of that type.

If the experimental determination of the overall size and shape of the polymer chain in flow is actually difficult, the observation of the deformation and orientation of individual parts of the chains should be even more problematic. So, in our Brownian dynamics simulations we decided to monitor the elongation and orientation of individual subchains with varying position along the chain, in order to grasp the aspect of the polymer molecule in the shear flow.

Theory and Methods

We consider a simple shear flow with shear rate $\dot{\gamma}$ in the x direction, with velocity components $v_x = \dot{\gamma}y$, and $v_y = v_z = 0$. The polymer model has N elements joined by $N - 1$ connectors. In an instantaneous conformation of the chain, the vector from the center of mass to the position of an element is denoted as $\mathbf{S}_i$ ($i = 1, ..., N$), and the connector vector joining elements j and $j + 1$ is denoted by $\mathbf{Q}_j$ ($j = 1, ..., N - 1$). The mean gyration (or inertia) tensor, $\langle \mathbf{SS} \rangle$ is defined as

$$\langle \mathbf{SS} \rangle = (1/N)\sum_i \langle \mathbf{S}_i \mathbf{S}_i \rangle \tag{1}$$

where $\langle ... \rangle$ indicates an average over polymer conformations in the shear flow. The diagonal terms of the gyration tensor, $\langle \mathbf{S}^2{}_{\alpha\alpha} \rangle$, with $\alpha = x, y, z$, characterize the average dimensions of the chain in the three main directions, and the mean-square radius of gyration, $\langle S^2 \rangle$, is simply the trace of $\langle \mathbf{SS} \rangle$

$$\langle S^2 \rangle = \langle S^2{}_{xx} \rangle + \langle S^2{}_{yy} \rangle + \langle S^2{}_{zz} \rangle \tag{2}$$

In the absence of flow the distribution of S_i is isotropic and therefore

$$\langle S^2{}_{xx} \rangle_0 = \langle S^2{}_{yy} \rangle_0 = \langle S^2{}_{zz} \rangle_0 = \langle S^2 \rangle_0/3 \tag{3}$$

where the equilibrium radius of gyration is given by

$$\langle S^2 \rangle_0 = (N^2 - 1)b^2/6N \tag{4}$$

$b^2 \equiv \langle Q^2{}_j \rangle_0$ is the square connector length at equilibrium and $\langle ... \rangle_0$ indicates the average over polymer conformations in the absence of flow ($\dot{\gamma} = 0$). The change in polymer dimensions due to the flow can be expressed for each

* To whom correspondence should be addressed.

0024-9297/92/2225-3574$03.00/0

direction, as the relative difference in $\langle S^2_{\alpha\alpha}\rangle$:

$$\phi_\alpha = \frac{\langle S^2_{\alpha\alpha}\rangle}{\langle S^2_{\alpha\alpha}\rangle_0} - 1 \tag{5}$$

and similarly for the whole radius of gyration

$$\phi = \frac{\langle S^2\rangle}{\langle S^2\rangle_0} - 1 \tag{6}$$

It follows from eqs 2–6 that

$$\phi = (\phi_x + \phi_y + \phi_z)/3 \tag{7}$$

The ϕ deformation ratios are functions of the shear rate. It is customary to use a dimensionless form of the shear rate, defined as

$$\beta = (M\eta_s[\eta]/N_A k_B T)\dot{\gamma} \tag{8}$$

As it has been demonstrated in previous works[12-14] (and indeed confirmed in our simulations), for long polymer chains and moderate shear rates, the polymer deformations depends on β following a simple square law. Denoting the proportionality constant as C, we have

$$\phi_\alpha = C_\alpha \beta^2 \tag{9a}$$

and

$$\phi = C\beta^2 \tag{9b}$$

with

$$C = (C_\alpha + C_\beta + C_\gamma)/3 \tag{10}$$

Thus, we can write

$$\langle s^2\rangle = \langle s^2\rangle_0(1 + C\beta^2) \tag{11}$$

and similar equations can be written for the three components.

Equations 9–11 are indeed valid both without and with hydrodynamic interaction (HI) (with different values for the constants), provided that the proper value is used for $[\eta]$ in eq 8. $[\eta]_{noHI}$ is trivially calculated,[15] while for $[\eta]_{HI}$ we use numerical values obtained by the Monte Carlo method.[16,17]

While the ϕ deformation ratios characterize numerically the extension of the polymer chain in the flow, a more intuitive image of the deformed chain can be grasped from the polar plot of the function[18,19]

$$l(\mathbf{u}) = ((1/N)\sum_{i=1}^{N}\langle(\mathbf{S}_i\mathbf{u})^2\rangle)^{1/2} \tag{12}$$

which gives a measure of the average size of the chain, l, in the direction of the unit vector $\mathbf{u}$. This function is experimentally relevant since the structure factor, $P(\theta)$, for low-angle scattering in an experiment in which the scattering vector is $\mathbf{q} = q\mathbf{u}$, with module q in the direction of $\mathbf{u}$, is given by

$$P(\theta) = 1 - q^2(l(\mathbf{u}))^2 + \ldots \tag{13}$$

Scattering data are often presented in the form of Zimm plots, in which reciprocals of intensities are plotted vs an angular variable containing q^2. The former are proportional to the reciprocal of the structural factor, given in the low-angle approximation by

$$P^{-1}(\theta) \simeq 1 + q^2(l(\mathbf{u}))^2 \tag{14}$$

Another aspect considered in this paper is the alignment of the polymer chain along the flow axis. An orientational order parameter can be defined for each connector in the chain

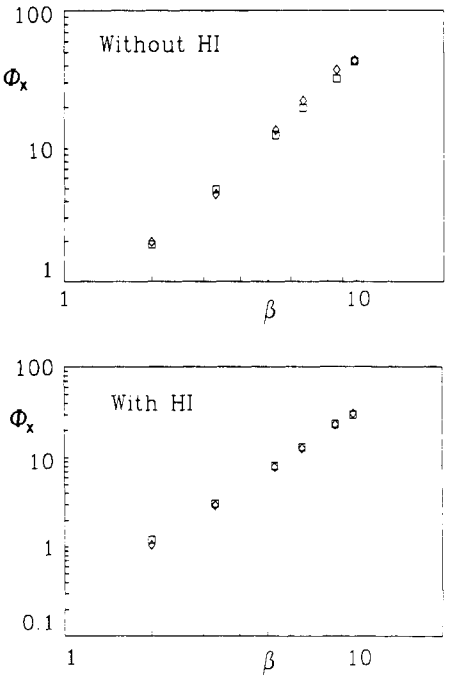

Figure 1. Deformation ratios ϕ_x for chains with and without HI: (□) $N = 12$; (◇) $N = 20$.

$$\langle P_2(j)\rangle \equiv \langle P_2(\cos\nu_j)\rangle = \langle(3\cos^2\nu_j - 1)/2\rangle \tag{15}$$

where ν_j is the angle subtended by the connector vector $\mathbf{Q}_j$ and the direction, x, of flow. In the absence of flow, the orientational distribution of the connectors is isotropic and $\langle P_2(j)\rangle_0 = 0$ while for very strong flows $\langle P_2(j)\rangle = 1$. The polymer solution, which must be isotropic at rest, is made anisotropic by the alignment of the polymer molecules in the flow and may become birefringent. This alignment of the whole chain can be measured as the average of the order parameter of the springs:

$$\langle P_2\rangle \equiv (1/N)\sum_i \langle P_2(i)\rangle \tag{16}$$

Our polymer model is a bead-and-spring chain of the Rouse type, with springs obeying Gaussian statistics at equilibrium. When HI effects are considered, we choose a specific Stokes radius for the beads of 0.256 in units of b, which gives a value for the hydrodynamic interaction $h^* = 0.25$. The chain length was $N = 12$ and 20. The Brownian dynamics simulation is carried out using the Iniesta–García de la Torre[20] second-order modification of the Ermak–McCammon algorithm[21] including solvent flow. Typically, the simulation had 10^6 steps of length $\Delta t = 0.02$ in units of $\zeta b^2/k_B T$ where ζ is the friction coefficient of the beads and $k_B T$ is Boltzmann's factor. The first part of the trajectory (2×10^5 steps for $N = 20$), during which the memory of the starting conformation is lost, is rejected in the computation of the averages. Of the remaining steps, one of each ten was used for the statistics. Quantities are handled in dimensionless form, as described previously. For instance, the dimensionless shear rate is

$$\dot{\gamma}^* = (6\pi\eta_s\sigma b^2/kT)\dot{\gamma} \tag{17}$$

This expression of shear rate should not be confused with the reduced (and also dimensionless) form in eq 8. In general, the working conditions are as in our previous papers,[4,6,7] where their validity was verified.

Table I
Square Radii of Gyration and Parameters of Chains of Different Length, with and without HI

$\dot{\gamma}^*$	β	$\langle S^2_{xx}\rangle$	$\langle S^2_{xy}\rangle$	$\langle S^2\rangle$	$\langle b^2(c)\rangle^a$	$\langle P_2(c)\rangle^a$	$\langle P_2\rangle$
			$N = 12$, without HI				
0.5	2	1.9	0.517	3.2	1.268	0.073	0.0451
0.82	3.3	3.9	0.846	5.2	1.539	0.1597	0.1018
1.32	5.3	8.9	1.361	10.0	2.223	0.29	0.197
1.65	6.6	19.7	1.701	15	2.851	0.3631	0.2555
2.15	8.6	22	2.216	24	4.066	0.4528	0.3328
2.47	9.9	29	2.546	31	5.012	0.51	0.38
			$N = 12$, with HI				
0.66	2	1.46	0.411	2.79	1.181	0.047	0.0326
1.1	3.3	2.7	0.665	4.1	1.355	0.1102	0.0770
1.76	5.3	6.0	1.072	7.9	1.809	0.214	0.16
2.2	6.6	9.3	1.360	10.6	2.261	0.2793	0.2416
2.86	8.6	16.3	1.844	17.7	3.239	0.3673	0.2827
3.3	9.9	21.8	2.122	23.1	4.047	0.415	0.317
			$N = 20$, without HI				
0.18	2	3.3	0.977	5.7	1.225	0.048	0.03
0.29	3.3	6.1	1.342	8.3	1.362	0.105	0.06
0.47	5.3	16.2	2.523	18.5	1.858	0.24	0.15
0.59	6.6	24.8	3.163	27.2	2.285	0.301	0.196
0.77	8.6	41.5	4.122	43.8	3.104	0.391	0.265
0.84	9.9	49.1	4.496	51.5	3.481	0.42	0.30
			$N = 20$, with HI				
0.3	2.0	2.28	0.642	4.39	1.182	0.0277	0.0188
0.5	3.3	4.4	1.074	6.6	1.356	0.0727	0.0463
0.8	5.3	9.9	1.773	12.0	1.810	0.148	0.1015
1.0	6.6	15.2	2.243	17.4	2.261	0.202	0.1411
1.3	8.6	27	3.069	30.2	3.240	0.2915	0.2036
1.5	9.9	35.4	3.384	37	4.047	0.34	0.23

[a] (c) indicates central bonds, with $j = N/2$.

Results and Discussion

Radius of Gyration. In Table I we present the main results of our simulations, obtained for two chain lengths, $N = 12$ and 20, and moderate shear rate, both without and with inclusion of HI. The results for $\langle S^2_{xx}\rangle$ show the elongation of the polymer in the direction of the flow. On the other hand, $\langle S^2_{yy}\rangle$ and $\langle S^2_{zz}\rangle$ (not shown) remained constant with increasing shear rate, within the statistical error of our simulations, being equal to the value in absence of the flow. In other words, $\phi_y \cong \phi_z \cong 0$ and the corresponding constants in the scaling law for the deformation rates (eq 9a) are obviously $C_y \cong C_z \cong 0$. Wang[14] has reported a result implying a quite small compression in the perpendicular directions, with $C_y = C_z = -0.69 \times 10^{-2}$, which is practically zero within the simulation uncertainty, in agreement with our calculations.

We have analyzed our $\langle S^2_{xx}\rangle$ and $\langle S^2\rangle$ data in terms of the scaling laws of the deformations ϕ_x and ϕ. Our results, plotted logarithmically in Figure 1 vs β, obey the square laws stated in eqs 9a,b. The least-squares-fitted slope in these plots is 1.9–2.1, with an unsignificant deviation from the theoretical exponent that may be attributed to statistical errors or to the finite chain lengths. The advantage of using β as a dimensionless form of the shear rate is that some results can be presented in a form independent of molecular weight (or chain length). This is indeed confirmed in Figure 1, where we can see that the results for $N = 12$ and $N = 20$ are practically coincident. Thus the longest chain used in our work seems to be sufficient and representative.

From our data, we obtain the following values for the deformation constants:

$$\text{HI:} \quad C_x = 0.29 \pm 0.02 \qquad C = 0.10 \pm 0.01 \qquad (18a)$$

$$\text{no HI:} \quad C_x = 0.45 \pm 0.02 \qquad C_x = 0.15 \pm 0.01 \qquad (18b)$$

The noHI value for C agrees perfectly with the theoretical prediction of Frisch et al.[13] In regard to the HI results, which are more relevant in the analysis of experimental data, we find that the HI values for C_x and C are in excellent agreement with the renormalization-group study of Wang.[14] (We note that Wang reported $C = 0.266$, when his correct result actually is $C = 0.09$, because he omitted the division by 3 in eq 10. We are grateful to Dr. S. Q. Wang for verifying this point.)

Unfortunately, experimental data on polymer deformation in shear flow are not abundant. The only experimental work available for comparison with these results is the multiple-orientation, low-angle neutron-scattering experiment of Linder and Oberthür.[10] Their deformation ratios, as the theoretical predictions, scale with β^2 for low β (say $\beta < 1$), while at larger β the exponent decreases, which is attributed by these authors to internal viscosity effects. They do not report a fitted value of the C constant, but from Figure 10 in ref 10 we estimate roughly $C = 0.15$–0.30. The large experimental errors in their deformation ratios do not allow a precise determination of C, but the result, anyhow, is not in agreement with the theoretical predictions, $C \cong 0.10$. As there is no doubt about the validity of the latter, which has been obtained by two independent, different techniques, the disagreement between theory and experiment remains to be explained. In addition to typical considerations about polydispersity and excluded volume, one would think of a possible lack of validity of the bead-and-spring model at high shear rates. The internal viscosity effect may also be important. Although we have not included all these additional effects in the present study, it should be pointed out that they can be adequately handled in Brownian dynamics simulations. Thus, we have already explored ways of introducing excluded volume interactions,[7,22] and internal viscosity can be simulated as described by Fixman.[23]

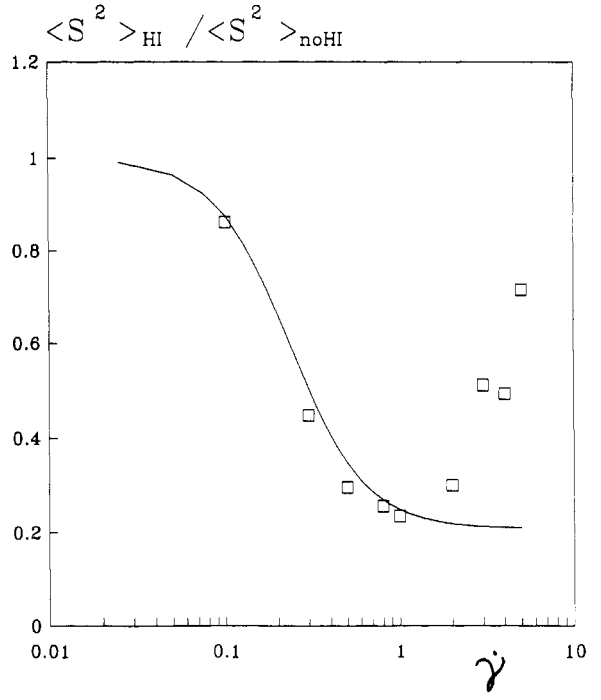

Figure 2. Ratio $\langle S^2\rangle_{HI}/\langle S^2\rangle_{noHI}$ vs shear rate $\dot{\gamma}^*$ for $N = 20$: (—) eq 19; (□) simulation.

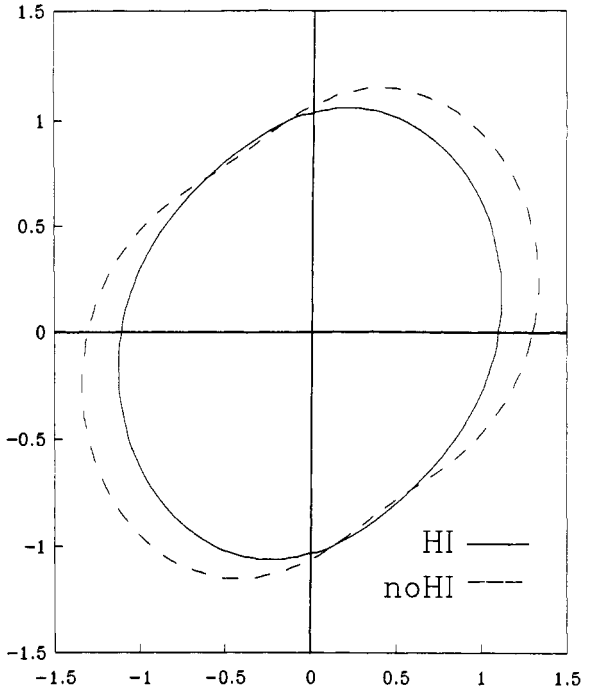

Figure 3. Polar plot of the shape function, $l(\mathbf{u})$ for $N = 20$ and a low shear rate, $\dot{\gamma}^* = 0.1$.

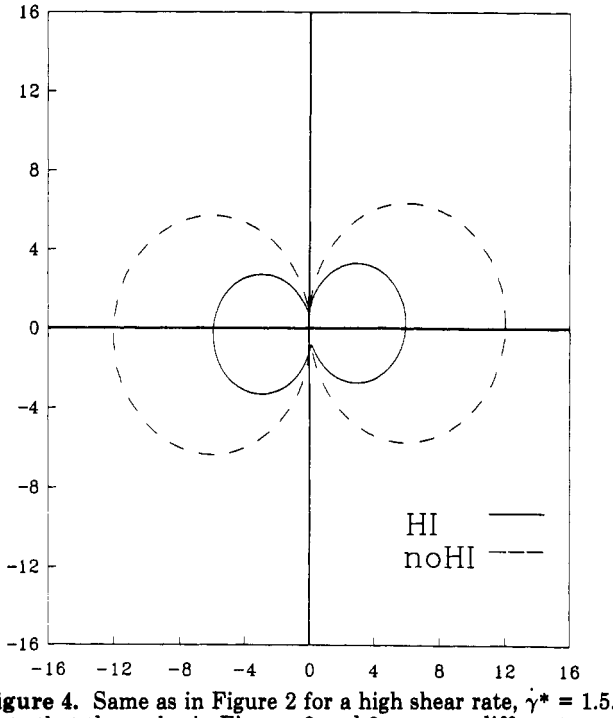

Figure 4. Same as in Figure 2 for a high shear rate, $\dot{\gamma}^* = 1.5$. Note that the scales in Figures 2 and 3 are very different.

By the way, we mention that Lindner and Oberthür compared their deformation ratios of the mean-square radius of gyration with theoretical predictions[23] for the *mean-square end-to-end distance*, $\langle r^2\rangle$, of bead-and-spring chains without HI (Rouse model) and with preaveraged HI (Zimm model). Apparently, their data followed better the Rouse model prediction, which is surprising due to the known importance of HI in polymer behavior. They implicitly assumed that the deformation ratios should be the same for the two properties. From our simulations, we have found that this is not true. The deformation ratios for $\langle r^2\rangle$ scale indeed with β^2, but the deformation constants (defined as in eqs 6 and 9b) are 0.21 (HI) and 0.13 (no HI), clearly different for those of $\langle S^2\rangle$. Thus, future experimental work should use, instead, the values in eq 18a.

The influence of HI in polymer dimensions may be relevant in the interpretation of experimental data. In our previous paper, from less precise simulation data and without the previous knowledge of the β^2 scaling law, we speculated that ϕ_{HI}/ϕ_{noHI}, and therefore $\langle S^2\rangle_{HI}/\langle S^2\rangle_{noHI}$, could tend to some constant value for a fixed shear rate $\dot{\gamma}$ with increasing polymer length. Now we see that this is not true. The ratio of the square radii is

$$\langle S^2\rangle_{HI}/\langle S^2\rangle_{noHI} = (1 + 0.09\beta^2{}_{HI})/(1 + 0.15\beta^2{}_{noHI}) \quad (19)$$

where we distinguish β_{HI} from β_{noHI}. In light of the chain length dependence of the intrinsic viscosity in both cases $[\eta]_{HI} \propto N^{1/2}$ and $[\eta]_{noHI} \propto N$, then $\beta_{HI} \propto N^{3/2}$, $\beta_{noHI} \propto N^2$, and therefore, $\langle S^2\rangle_{HI}/\langle S^2\rangle_{noHI} \propto N^{-1}$. Thus, the polymer is smaller due to HI, and the difference is larger for longer polymers.

As kindly noted by a referee, eq 19 incorrectly predicts that $\langle S^2\rangle_{HI}/\langle S^2\rangle_{noHI} \to 0$ for very high shear rates (fixed N and $\dot{\gamma} \to \infty$), whilst one expects from physical intuition that, in such a limit, the chain is very stretched, HI effects vanish and therefore $\langle S^2\rangle_{HI}/\langle S^2\rangle_{noHI} \to 1$. This puzzling behavior of eq 19 is due to the fact that it is not valid in that limit, when $\beta \to \infty$. Actually, in addition to the results in Table I, we obtained results (not listed) for higher shear rates, up to $\dot{\gamma} = 5$, for which $\langle S^2\rangle$ is about 300 times larger than $\langle S^2\rangle_0$. The ϕ deformations seem to follow the β^2 law in the no-HI case, but when HI is included, a systematic upward curvature is found and eqs 11 and 19 fail. In Figure 2 we present a set of results including those at high $\dot{\gamma}$. As predicted by eq 19, $\langle S^2\rangle_{HI}/\langle S^2\rangle_{noHI}$ decreases with increasing $\dot{\gamma}$ at low $\dot{\gamma}$, obeying eq 19. At intermediate $\dot{\gamma}$, eq 19 is no longer valid and the simulation results show a minimum, after which the ratio increases, suggesting the correct $\langle S^2\rangle_{HI}/\langle S^2\rangle_{noHI} \to 1$ limit.

Shape Function and Scattering. The components of the radius of gyration tensor are used to plot the shape function $l(\mathbf{u})$. Two examples, corresponding to low and high shear rates, are displayed in Figures 3 and 4. In order to focus on polymer shape, the scales in those figures are widely different, so that different polymer sizes are presented in a plot of similar size. For $\dot{\gamma} = 0$, the plot should be a circle of radius equal to $(\langle S^2\rangle_0/3)^{1/2}$ (1.05 for

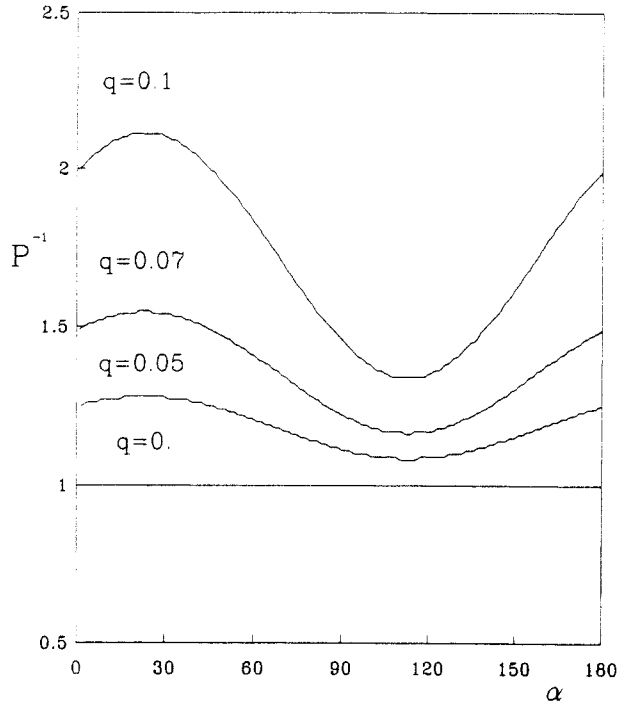

Figure 5. Scattering intensity structure factor at scattering vectors with the indicated moduli, that make an angle α with the direction of flow. Results are for a M = 170 000 polystyrene in oligostyrene/toluene at $\dot{\gamma}$ = 9680 s^{-1}.

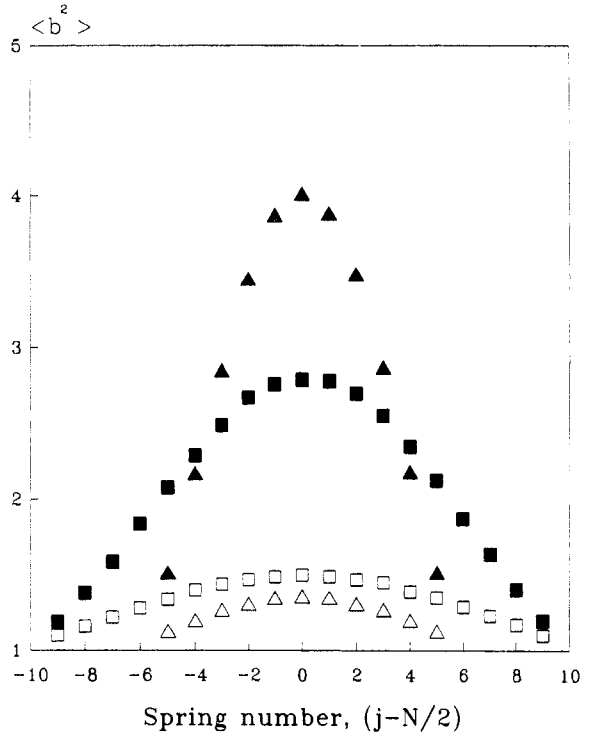

Figure 6. Mean-squared bond length of the individual springs, $\langle b^2_i \rangle$, as a function of their position along the chain: (■) N = 20, $\dot{\gamma}^*$ = 1.5, β = 9.9; (▲) N = 12, $\dot{\gamma}^*$ = 3.3, β = 9.9; (□) N = 20, $\dot{\gamma}^*$ = 0.8, β = 5.3; (△) N = 12, $\dot{\gamma}^*$ = 1.5, β = 5.3. Springs are numbered here from the center. Results are with HI.

N = 20). The anisometry is evident even for the lowest $\dot{\gamma}$. We note that at low shear rates the maximum measure of the polymer is along a direction making some angle with the flow axis, roughly 45° in Figure 3, while at high shear rate the longest elongation takes place along the flow axis, as in Figure 4.

As the $l(\mathbf{u})$ function has not been experimentally achieved as yet, it is interesting to predict results in real conditions. Mimicking conditions in the neutron-scattering experiment by Lindner and Oberthür,[10] we assume a solution of polystyrene with M = 170 000 in the solvent mixture olygostyrene/toluene, with $\langle S^2 \rangle_0$ = 12.1 nm at rest. We model the polymer chain as a bead-and-spring chain with N = 20 (this choice should be irrelevant for the present purpose, provided that N is high enough). In the absence of flow, the root-mean-square length of the springs should be then b = 6.6 nm. The shear rate is taken as $\dot{\gamma}$ = 9680 s^{-1}, which corresponds to β = 5.3[10] and to $\dot{\gamma}^*$ = 0.3 in our reduced units. From our results in Table I, $\langle S^2 \rangle / \langle S^2 \rangle_0$ = 3.6, and the size of the polymer in the sheared solution is roughly twice that of the one at rest. We take two values for the modulus of the scattering vector: q = 0.05 nm^{-1} and q = 0.10 nm^{-1}. The first one is the lowest used in ref 10, and the second one is still in the low-angle region where the linearity with q^2 in eq 14 holds. Then, we proceed to calculate the $l(\mathbf{u})$ function as described above, and the results are substituted into eq 14 to calculate the reciprocal of the scattering structure factor, $P^{-1}(q)$, which can be interpreted as the reciprocal of the intensity of scattered radiation in some units, at scattering vector q. This vector makes an angle, α, with the direction of flow. In Figure 5 we present the dependence of scattering intensity on α for the two q's. It is evident that the intensity presents a remarkable variation with α (even for small values of q) that could be observed experimentally.

Deformation and Orientation of Springs. All the results reported insofar are relative to the overall shape and orientation of the polymer chain. It is interesting to look at the deformation and orientation of individual subchains, represented in the model by individual springs, in order to have a more detailed view of the conformation in the flow. In Figure 6 we show how the square spring length, $\langle b^2_i \rangle$, varies with the position of the bond along the chain. There is a well-pronounced maximum at the central spring, and the sharpness of the maximum does not seem to decrease with increasing chain length. Thus we discard the possibility of a uniform expansion in the center of the chain; instead, the elongation of individual subchains increases smoothly from the end toward the center of the polymer.

We have tried a scaling-law representation of the stretching of the springs, choosing for that purpose the central one. In the logarithmic plot in Figure 7, we present the deformation ratios for $\langle b^2_c \rangle$ (c = 10 for N = 20 and c = 6 for N = 12), given as usual by $\langle b^2_c \rangle / \langle b^2_c \rangle_0 - 1$, as functions of shear rate. We observe that the bond deformation scales with $\dot{\gamma}^2$, as the overall dimensions did, but only for high shear rates, while for the latter this behavior was observed at low rates also. Another difference is that, when shear rates are expressed in the β form, the data for different N with fixed HI conditions do not superimpose, which indicates that the β representation is not appropriate for individual subchains.

The other aspect regarding individual subchains or springs is their orientation in the flow, measured by the $\langle P_2(j) \rangle$ values as defined in eq 15. Their variation along the chain is illustrated in Figure 8, in the same form as in Figure 6 for the spring length. The aspects of both curves are similar, so that the alignment of the subchains along the flow is more intense at the very center of the chain and decreases smoothly toward the end. The $\langle P_2 \rangle$ values for the whole chain, as defined in eq 16, are listed in Table I. We note that the shear-rate dependence of $\langle P_2 \rangle$, when the rate is expressed in terms of β, is clearly dependent on N. In other words, the β representation of the shear-rate dependence, which was very useful for the description

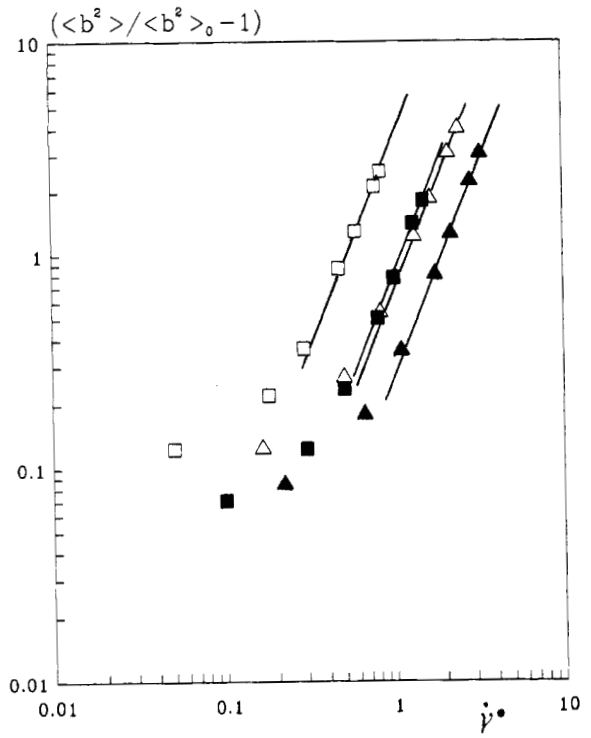

Figure 7. Deformation ratio for the central bond plotted logarithmically vs shear rate: (■) $N = 20$, HI; (□) $N = 20$, no HI; (▲) $N = 12$, HI; (△) $N = 12$, no HI.

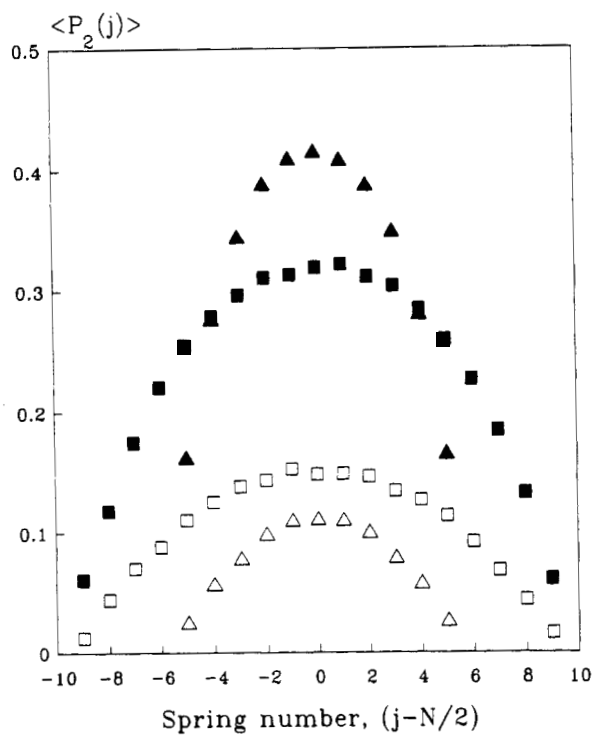

Figure 8. Same as in Figure 6 for the order parameter of the bonds in the chain.

of polymer dimensions, seems not to be valid for orientation. The alignment of the polymer molecules in a shear flow may be manifested by the technique of flow birefringence. This property, from the point of view of a bead-and-spring model, depends in a simultaneous and complex way on the stretching of the subchains (which changes their optical anisotropy) as well as their orientation. The Brownian dynamics simulation technique used in this work is a promising procedure for future studies of flow birefringence and other properties.

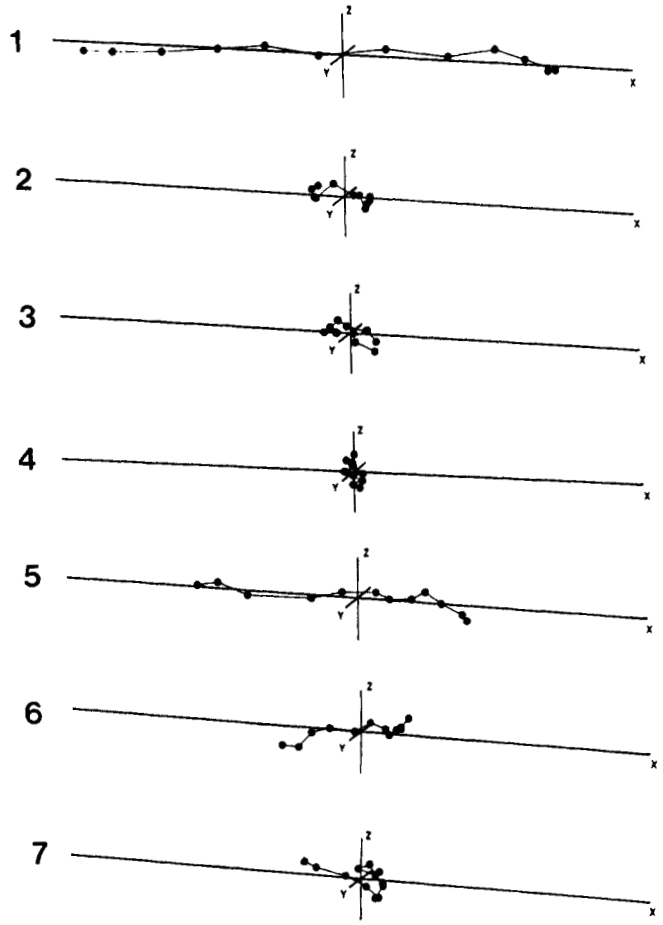

Figure 9. Snapshots of a chain with $N = 12$ in a shear flow with $\gamma = 3.3$, taken from a BD trajectory of 10^6 steps. Snapshot 1 was taken after 4×10^5 steps, and the following ones at regular intervals of 10^5 steps.

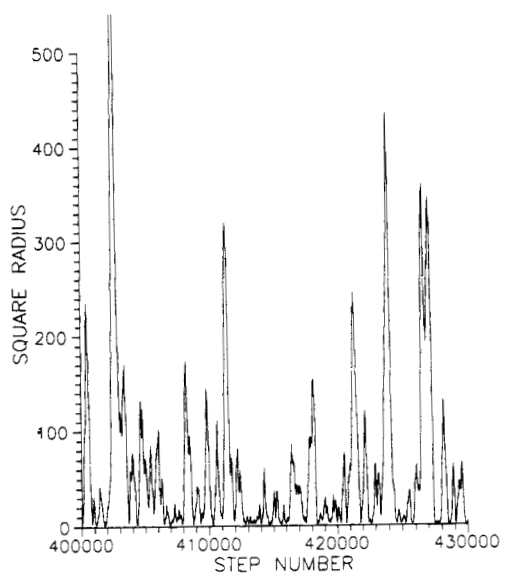

Figure 10. Trace of the instanteous value of S^2 along a portion of 30 000 steps of the trajectory for $N = 12$ and $\gamma^* = 3.3$. Under these conditions, $\langle S^2 \rangle = 59$.

In addition to all the numerical results presented so far, an intuitive knowledge of the chain conformation can be grapsed from a set of snapshots of the chain, which is shown in Figure 9. The aspect of these snapshots is very similar to that presented by Liu for another chain model.[3] In our opinion, the main feature in this view is the variability of the chain conformation. Instead of being continuously more or less stretched and oriented along the flow, we see that the chain fluctuates between

conformations (like 1) that are very elongated and oriented, with an instantaneous S^2 which may be much larger than the mean, $\langle S^2 \rangle$, and other conformations that resemble the random coil that we would observe in the absence of flow. In Figure 9, the successive snapshots are separated by a large number of steps, so that they can be considered as a set of representative, statistically independent conformations. It is interesting to know the rate of such conformational fluctuations. This is illustrated by the trace of S^2 along a small portion of the trajectory, plotted in Figure 10, which shows the alternation between the very stretched and very coiled states. The typical time for transition (width of the peaks in Figure 10) is about 10^3 steps, i.e., 20 units of reduced time. This is of the same order as the first relaxation time of the chain under those conditions. A detailed and quantitative characterization of the fluctuations of the chain conformations in shear flow, using both experimental dynamic techniques and Brownian dynamics simulations would be most interesting.

Acknowledgment. This work was supported by Grant PB87-0694 from the Direccion General de Investigacion Cientifica y Tecnica (MEC) and Grant PB90/20 from the Direccion General de Educacion y Universidad (Region de Murcia). J.J.L.C. acknowledges a predoctoral fellowship from the Plan de Formacion de Personal Investigador.

References and Notes

(1) Dotson, P. *J. Chem. Phys.* **1983**, *79*, 5730.
(2) Saab, H. H.; Dotson, P. J. *J. Chem. Phys.* **1987**, *86*, 3039.
(3) Liu, T. W. *J. Chem. Phys.* **1989**, *90*, 5826.
(4) Díaz, F. G.; García de la Torre, J.; Freire, J. J. *Polymer* **1989**, *30*, 259.
(5) Zylca, W. Öttinger, H. C. *J. Chem. Phys.* **1989**, *90*, 474.
(6) López Cascales, J. J.; García de la Torre, J. *Macromolecules* **1990**, *23*, 809.
(7) López Cascales, J. J.; García de la Torre, J. *Polymer* **1992**, *32*, 3359.
(8) Zylka, W. *J. Chem. Phys.* **1991**, *94*, 4628.
(9) López Cascales, J. J.; García de la Torre, J. *J. Chem. Phys.* **1991**, *95*, 9384.
(10) Lindner, P.; Oberthür, R. C. *Colloid Polym. Sci.* **1988**, *266*, 886.
(11) Bird, R. B.; Saab, H. H.; Dotson, P. J.; Fan, X. J. *J. Chem. Phys.* **1983**, *79*, 5729.
(12) Pistoor, N.; Binder, K. *Colloid Polym. Sci.* **1988**, *266*, 132.
(13) Frisch, H. L.; Pistoor, N.; Sariban, A.; Binder, K.; Fesjian, S. *J. Chem. Phys.* **1989**, *89*, 5194.
(14) Wang, S. Q. *J. Chem. Phys.* **1990**, *92*, 7618.
(15) Bird, R. B.; Curtiss, C. F.; Armstrong, R. C.; Hassager, O. *Dynamics of Polymeric Liquids. Kinetic Theory*; Wiley: New York, 1977; Vol. 2.
(16) Tirado, M. M.; López Martínez, M. C.; García de la Torre, J.; Freire, J. J. *Macromolecules* **1984**, *172*, 2715.
(17) García de la Torre, A. Jimenez; Freire, J. J. *Macromolecules* **1982**, *15*, 148.
(18) Roitman, D. B.; Schrag, J. L. In *Polymer-Flow Interaction*; Rabin, Y., Ed.; American Institute of Physics Conference Proceedings, No. 137; AIP: New York, 1985; p 77.
(19) Hoagland, D. A. *Macromolecules* **1987**, *20*, 2633.
(20) Iniesta, A.; García de la Torre, J. *J. Chem. Phys.* **1990**, *92*, 2015.
(21) Ermak, D. L.; McCammon, J. A. *J. Chem. Phys.* **1978**, *69*, 1352.
(22) Rey, A.; Freire, J. J.; García de la Torre, J. *Polymer*, in press.
(23) Fixman, M. *J. Chem. Phys.* **1988**, *89*, 2442.
(24) Peterlin, A. *J. Chem. Phys.* **1963**, *39*, 224.

Registry No. Polystyrene (homopolymer), 9003-53-6; neutron, 12586-31-1.